Interfacial Slip in Entrained Soap Films Containing Associating Hydrosoluble Polymer

Eric A. Adelizzi and Sandra M. Troian*

Microfluidic Research & Engineering Laboratory, Department of Chemical Engineering, Princeton University, Princeton, New Jersey 08544

Received August 12, 2003. In Final Form: March 6, 2004

Frankel's law predicts that the thickness of a Newtonian soap film entrained at small capillary number scales as $Ca^{2/3}$ provided the bounding surfaces are rigid. Previous studies have shown that soap films containing low concentrations of high molecular weight (M_w) polymer can exhibit strong deviations from this scaling at low *Ca*, especially for associating surfactant−polymer solutions. We report results of extensive measurements by laser interferometry of the entrained film thickness versus *Ca* for the associating pair SDS/PEO over a large range in polymer molecular weight. Comparison of our experimental results to predictions of hydrodynamic models based on viscoelastic behavior shows poor agreement. Modification of the Frankel derivation by an interfacial slip condition yields much improved agreement. These experiments also show that the slip length increases as M_w^{ζ} where $\zeta = 0.58 \pm 0.07$. This correlation is suggestive of the Tolstoi−Larsen prediction that the slip length increases in proportion to the characteristic size of the fluid constituent despite its original derivation for liquid−solid interfaces.

I. Introduction

Soap films, especially the brilliant interference patterns they display, never fail to fascinate. Despite how easy it is to form such films, predictions of their equilibrium shapes require study of minimum energy surfaces. Through the years, however, combinations of analytic work and software packages such as *Surface Evolver*[1] have effectively mapped out the many allowed static shapes that can form on supporting frames. By contrast, there still remain open questions involving the formation and dynamic behavior of soap films. Even a simple setup in which a wire frame is withdrawn from a reservoir containing a pure soap solution produces complex border instabilities that are not well-understood. To complicate matters, most industrially or biologically relevant films do not consist of solutions of pure water and surfactant. Alcohols, polymers, and even glass beads are often added to help stabilize films against premature rupture to produce high-quality foams and emulsions. Polymeric additives can undergo association with surfactant micelles to generate non-Newtonian behavior. In addition, these large aggregates are confined to slender geometries since typical soap films range in thickness from tens of micrometers to tens of angstroms. Such confinement can give rise to anisotropic behavior and layering phenomena, especially when the aggregate size approaches the length scale of the film thickness.

The behavior of microstructured fluids in confined geometries can be investigated with high-resolution experimental tools, such as light or neutron scattering, which measure aggregate size, conformational changes, and local ordering effects. Unfortunately, the results of such measurements are difficult to incorporate directly into hydrodynamic models for the prediction of macroscopic behavior. Our interest here lies with larger scale phenomena that can be probed through hydrodynamic and rheological measurements. We seek to characterize the collective behavior of associating polymers and surfactant micelles through a hydrodynamic analysis which relies on a minimal set of parameters.

Especially problematic to the comparison between experimental results and predictions of hydrodynamic models is the issue of boundary conditions at the gas−liquid interface. Mysels et al. first distinguished three types of films based on observations of the colored interference fringes and swirling patterns at the film surface. He classified films as either rigid (immobile), simple mobile, or irregular mobile[2] depending on the degree and uniformity of the surface motion. Small markers on the surface of immobile films showed no relative motion. Generally speaking, surfactant solutions above the critical micelle concentration (CMC) and solutions containing cosurfactant additives such as glycerol typically produce thicker films with rigid interfaces. By contrast, solutions below the CMC often exhibit significant fluid motion and swirling at the gas−liquid interface. These mobile films are normally much thinner and drain at a much faster rate than rigid films. The surface motion of mobile films is attributed to inhomogeneities in the surface surfactant concentration which produce Marangoni stresses.[3−5] Rigid surfaces, by contrast, contain an abundance of surfactant which leads to rapid equilibration of any surface concentration inhomogeneities. Real soap films do not fall neatly into any one category and can display intermediate character depending on the time scales relevant to adsorption and desorption of the surfactant compared to the entrainment or convective process. The focus of this current work is how an effective slip condition at the gas−liquid interface can be used to parametrize the soap film entrainment process in associating polymer−surfactant solutions above the CMC.

A. Frankel's Law. Mysels et al.[2] were the first to propose for rigid Newtonian films a relation between the

* Corresponding author. E-mail: stroian@princeton.edu.

(1) Brakke, K. *Exp. Math.* **1992**, *1*, 141.

(2) Mysels, K. J.; Shinoda, K.; Frankel, S. *Soap Films: Studies of Their Thinning*; Pergamon Press: New York, 1959; Chapter 5.

(3) Schwartz, L. W.; Roy, R. V. *J. Colloid Interface Sci.* **1999**, *218*, 309.

(4) Nierstrasz, V. A.; Frens, G. *J. Colloid Interface Sci.* **1998**, *207*, 209.

(5) Breward, C. J. W.; Howell, P. D. *J. Fluid Mech.* **2002**, *458*, 379.

10.1021/la035480x CCC: $27.50
Published on Web 07/28/2004

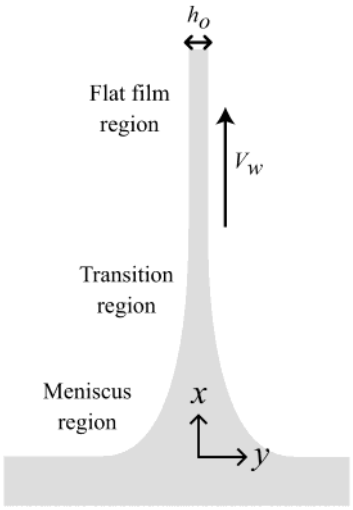

Figure 1. Schematic diagram of a soap film entrained at constant speed V_w. The x axis signifies the direction of film withdrawal; the y axis lies parallel to the reservoir interface. The limiting film thickness is h_0.

entrained film thickness, h_0, and the capillary number $Ca = \mu V_w/\gamma$, where μ is the liquid viscosity, γ the surface tension, and V_w the film withdrawal speed for $Ca \ll 1$. The schematic diagram in Figure 1 depicts a cross-sectional view of the model entrainment process with three important regimes noted. The quantity h_0 represents the uniform film thickness far from the meniscus region where the velocity profile, governed by viscous forces, is everywhere pluglike, that is, $u(x, y) = V_w$. At the opposite end and in the limit $Ca \ll 1$, he assumed that the meniscus curvature, governed by the balance of capillary and hydrostatic forces, would remain equal to its static value $\kappa = \sqrt{2\rho g/\gamma}$ where ρ is the liquid density and g the gravitational constant. These two regions ($x \rightarrow \infty$ and $x \rightarrow 0$) were made to conform smoothly to the curved shape defining the transition region governed by the balance of viscous and capillary forces by solving the relevant interfacial equation subject to the boundary conditions established by the two extremes. The velocity profile in the transition region was shown to correspond to a linear superposition of Poiseuille flow (caused by capillary drainage) and Couette flow (caused by the entrainment process). The Frankel derivation was restricted to rigid films; that is, the boundary conditions at the free surfaces were assumed to be $u(x, y)|_{y=\pm h(x,t)} = V_w$. Within these approximations, the relation between the dimensionless film thickness H and the capillary number was determined to be

$$H = \frac{h_0}{\sqrt{\gamma/\rho g}} = 1.89Ca^{2/3} \qquad (1)$$

a relation now known as Frankel's law.[6,7]

A very similar approach has been used by others to compute the entrained film thickness for a number of different problems including a rigid plate[8] and cylindrical wire[9,10,11] withdrawn from a solution at constant speed as well as a bubble translating at constant speed within a smooth capillary tube.[12] While the exponent of the capillary number remains fixed at 2/3 (provided the approximations remain valid), the numerical prefactor and the characteristic length scale used to nondimensionalize the film thickness can change with system geometry. Geometries which introduce a second curvature comparable to the meniscus curvature[13] can reduce the exponent from 2/3 to 1/3. Matched asymptotic analyses[14] and comparison to experiments[15] have established the validity of eq 1 for $Ca \lesssim 0.01$.

B. Experimental Deviations from Frankel's Law. Experimental confirmation of Frankel's law has been obtained with a variety of aqueous surfactant solutions.[7] More recent studies have focused on deviations obtained with associating polymer−surfactant solutions. For example, aqueous solutions of poly(ethylene oxide) (PEO) and sodium dodecyl sulfate (SDS) are known to form polymer−micelle complexes.[16−21] The addition of SDS in the range 2−46 mM to aqueous PEO solutions (0.25 wt %, $M_w = 5 \times 10^6$) causes a significant increase in the viscosity with increasing shear rate. This enhancement, which is most significant above the critical concentration for formation of polymer-bound micelles, is observed to level off at the saturation concentration where the maximum number of micelles is bound to the polymer chain. This observation has led to the hypothesis that coil expansion of PEO caused by the binding of SDS micelles to the polymer backbone creates microstructured complexes. Such mixtures are well-characterized as power-law fluids, especially at higher SDS concentrations.[19]

The behavior of soap films consisting of associative complexes has not been studied extensively. Cohen-Addad and di Meglio were the first to characterize the entrained film thickness at small capillary number for solutions containing various polymer−surfactant pairs including SDS/PEO.[22−24] Their studies were restricted to two molecular weights, namely, $M_w = 100$K and 4M PEO, and SDS concentrations above the CMC. The 100K PEO/SDS solutions showed no discernible deviation from Frankel's law; strong deviations were evident for the 4M PEO/SDS, even at polymer concentrations as low as 0.05 wt %. At the smallest values of Ca, the films were much thinner than Frankel's prediction. At the highest values of Ca, the film thickness saturated to a value equal to or slightly larger than the diameter of the fibers used to support the film. The entrained film thickness[24] of solutions containing 4M PEO/SDS was found to obey the correlation $H \sim Ca^2$ and not $H \sim Ca^{2/3}$.

C. Parametrization by Interfacial Slip. A number of theoretical models have been proposed to explain the deviations from Frankel's law at the lower range in Ca observed in SDS/PEO films. Viscoelastic effects can strongly modify hydrodynamic behavior, thereby affecting the correlation between the entrained film thickness and

(6) Mysels, K. J.; Cox, M. C.; Skewis, J. D. *J. Phys. Chem.* **1961**, *65*, 1107.
(7) Mysels, K. J.; Cox, M. C. *J. Colloid Interface Sci.* **1962**, *17*, 136.
(8) Landau, L.; Levich, B. *Acta Physicochim. U.R.S.S.* **1942**, *17*, 42.
(9) Goucher, F. S.; Ward, H. *Philos. Mag.* **1922**, *44*, 1002.
(10) White, D. A.; Tallmadge, J. A. *AIChE J.* **1966**, *12*, 333.
(11) Quéré, D.; de Ryck, A. *Ann. Phys. Fr.* **1998**, *23*, 1.
(12) Bretherton, F. P. *J. Fluid Mech.* **1961**, *10*, 166.
(13) Darhuber, A. A.; Troian, S. M.; Davis, J. M.; Miller, S. M. *J. Appl. Phys.* **2000**, *88*, 5119.
(14) Wilson, S. D. R. *J. Eng. Math.* **1982**, *16*, 209.
(15) Probstein, R. F. *Physicochemical Hydrodynamics, 2nd ed.*; J. Wiley & Sons: New York, 1994; Chapter 10.
(16) Jones, M. N. *J. Colloid Interface Sci.* **1967**, *23*, 26.
(17) Schwuger, M. J. *J. Colloid Interface Sci.* **1973**, *43*, 491.
(18) Cabane, B. *J. Phys. Chem.* **1977**, *81*, 1639.
(19) Brackman, J. C. *Langmuir* **1991**, *7*, 469.
(20) Brown, W.; Fundin, J.; Miguel, M. *Macromolecules* **1992**, *25*, 7192.
(21) Cooke, D. J.; Dong, C. C.; Lu, J. R.; Thomas, R. K.; Simister, E. A.; Penfold, J. *J. Phys. Chem. B* **1998**, *102*, 4912.
(22) Lionti-Addad, S.; di Meglio, J.-M. *Langmuir* **1992**, *8*, 324.
(23) Cohen-Addad, S.; di Meglio, J.-M. *Langmuir* **1994**, *10*, 773.
(24) Cohen-Addad, S. *Films mixtes de savon et de polymére.* Ph.D. Thesis, L'Université Paris VI, 1992.

Ca. As shown in section IV, however, none of the rheological models so far proposed show satisfactory agreement with experiment.

In this work, similar laser interferometry experiments as described previously[22,23] are used to examine the entrained film thickness of aqueous SDS/PEO solutions over a wider range in molecular weight (from 17.5K to 8M). Independent measurements of the shear-dependent viscosity and normal stress coefficients help establish that the solutions behave as Newtonian liquids at the shear rates relevant to the entrainment process. Direct comparison of the measured entrained film thickness to hydrodynamic models assuming shear thinning or Oldroyd B type behavior shows poor agreement. Surprisingly, extension of Frankel's analysis for Newtonian films to include an interfacial slip boundary condition as a way of mimicking the behavior of mobile surfaces yields good agreement over the range in *Ca* of interest. The inferred slip lengths are shown to increase with polymer molecular weight according to M_w^a where $a = 0.58 \pm 0.07$. This correlation is suggestive of the Tolstoi−Larson prediction[25−27] that the slip length increases in proportion to the characteristic size of the fluid constituent despite its original derivation for liquid−solid interfaces. Without further study, it is not yet possible to determine whether the effective slip behavior reflects the formation of Marangoni stresses due to surface compositional inhomogeneities associated with polymer−surfactant aggregates[3,4] or whether there exists real slippage between the interior and surface layers of the suspended complexed film.

II. Experimental Details

A. Materials. The two (anionic) surfactants used in this study were SDS ($C_{12}H_{25}O_4SNa$) (99%, Aldrich) and SDBS ($C_{12}H_{25}C_6H_4SO_3Na$, technical grade, Aldrich). Glycerol ($C_3H_8O_3$, 99.5%, Aldrich) was added to pure aqueous SDS solutions to form rigid soap films.[6,7,28,29] The SDBS solutions seem naturally to produce rigid films with no additives. The molecular weights of PEO ($[(CH_2)_2O]_n$, nonionic surfactant) ranged from 17.5K to 8M. The polymers were all used as received (Aldrich, Fluka, Alfa Aesar). Doubly deionized water (18 MΩ-cm, Hydro Ultrapure) was used to prepare all solutions. The solutions were gently stirred for a minimum of 24 h to maximize solubilization. The high M_w PEO solutions required several days of stirring for complete dissolution. All solutions were then placed in a cleaned glass cell, degassed under vacuum, and sealed until further use. For these studies, the surfactant concentration was held fixed at 2 wt %, well above the critical micelle concentration (0.25 wt % for aqueous SDS solutions and 0.17 wt % for aqueous SDBS solutions at room temperature and without polymer).[30] The polymer concentration varied from about 0.04 to 5.0 wt %.

B. Solution Characterization. The surface tension of all solutions was measured by the Wilhelmy method using a small platinum plate, which was flame-cleaned, rinsed in ultrapure water, and dried in a filtered nitrogen stream before each measurement. A Denver Instrument balance (Model A160, 0.1-mg limit) with a resolution of ±0.03 mN/m was used to measure the force on the platinum plate. The addition of PEO to pure aqueous SDS solutions caused a small increase in the surface tension, indicating some adsorption of the PEO to the air−liquid interface. This absorption seems to prevent the formation of swirling flow patterns at the film surface, as sometimes observed in pure aqueous SDS solutions.

Table 1. Measured Surface Tension, γ, and Measured Zero-Shear Viscosity, μ, for All Solutions Used in This Study[a]

solution (wt %)	γ (mN/m)	μ (cP)	c^* (wt %)	$\dot{\gamma}$ (s^{-1})
2% SDBS	29.4	1		8−250
2% SDS	37.3	1		N/A
with 2% glycerol	36.7	1		5−450
4% glycerol	36.2	1		10−250
2% 17.5K PEO	39.2	3	6.2	5−30
5% 17.5K PEO	38.9	10	6.2	1.5−25
3% 100K PEO	37.1	13	2.6	0.9−10
1.5% 200K PEO	37.1	10	1.8	2−75
2% 400K PEO	37.9	69	1.2	0.4−10
0.5% 1M PEO	37.5	130	0.8	0.3−120
0.15% 4M PEO	36.2	103	0.4	1−400
0.044% 8M PEO	36.4	43	0.3	0.4−5

[a] The range in shear rates produced during film entrainment was estimated according to $\dot{\gamma} \approx 2V_w/h_0$, where the total film thickness is h_0. The polymer overlap concentration c^* (assuming no surfactant), based on the estimate provided by eq 2 with $f = 3/4\pi$, is listed in the second-to-last column.[32] Concentrations are all quoted in weight percent.

The index of refraction of all solutions was obtained with an ECCI Scientific Abbe refractometer with resolution ±0.0003. The values ranged from $n = 1.333$ (pure water) to $n = 1.338$ (surfactant−polymer solutions). The index of refraction of these liquid samples was used to calculate the film thickness from the interferometry data. Corrections to these measurements based on a treatment of the soap film as a layered structure with different indices of refraction have been shown to be negligible and were therefore ignored.[28]

The zero-shear bulk viscosity of solutions was measured with a falling ball viscometer. Curves of the shear-dependent viscosity were either obtained with a Rheometrics Ares HR Rheometer in a cone and plate configuration or a Rheometrics RFS II Couette Rheometer. The Rheometrics Ares HR instrument was equipped with transducers to measure normal forces. With a gap spacing of 50 μm and an opening cone angle of 0.04 rad, the shear rates accessible with this instrument ranged from 0.1 to 1000 s^{-1}.

Table 1 lists the measured values of the surface tension and zero-shear viscosity for all solutions used in this study. It was not possible to form films with high M_w PEO while keeping the polymer concentration constant since the solutions were often too viscous. For each M_w studied, we chose a sufficiently high polymer concentration that would still allow formation of a stable film. Estimates of the critical overlap concentration c^*, for a polymer in a good solvent[27] (with no surfactant), are also given in Table 1. The overlap concentration was determined from the relation[31,32]

$$c^* \approx f \frac{M_w}{N_A R_g^3} \tag{2}$$

where N_A is Avogadro's number and $f = 3/4\pi$. The prefactor f is sometimes eliminated altogether[32] or set to a value of 1/8 depending on the model used.[33] This estimate provides only a rough value of the concentration at which polymer chains in solution, modeled as Gaussian coils, will overlap. The polymer concentrations in our study (Table 1) were all close to the estimated value of c^*. The presence of surfactant is expected to modify the behavior, size, and interactions of the polymer coils, especially in cases where it can associate with surfactant micelles. SDS, for example, is known to increase the effective radius of gyration of PEO in water.[34,35]

The last column in Table 1 contains an estimate of the effective shear rates $\dot{\gamma}$ in the suspended film during the entrainment

(25) Tolstoi, D. M. *Dokl. Acad. Nauk. SSSR* **1952**, *85*, 1089.
(26) Blake, T. D. *Colloids Surf.* **1990**, *47*, 135.
(27) Larson, R. G. *The Structure and Rheology of Complex Fluids*; Oxford University Press: New York, 1999.
(28) Lyklema, J.; Scholten, P. C.; Mysels, K. J. *J. Phys. Chem.* **1965**, *69*, 116.
(29) Lyklema, J. *Rec. Trav. Chim. Pays-Bas* **1962**, *81*, 890.
(30) Porter, M. R., Ed. *Handbook of Surfactants, 2nd. ed.*; Blackie Academic and Professional: New York, 1994.
(31) Fujita, H. *Polymer Solutions*; Elsevier: New York, 1990.
(32) Ying, Q.; Chu, B. *Macromolecules* **1987**, *20*, 362.
(33) Graessley, W. W. *Polymer* **1980**, *21*, 258.
(34) Francois, J.; Dayantis, J.; Sabbadin, J. *Eur. Polymer J.* **1985**, *21*, 165.
(35) Chari, K.; Antalek, B.; Lin, M. Y.; Sinha, S. K. *J. Chem. Phys.* **1994**, *100*, 5294.

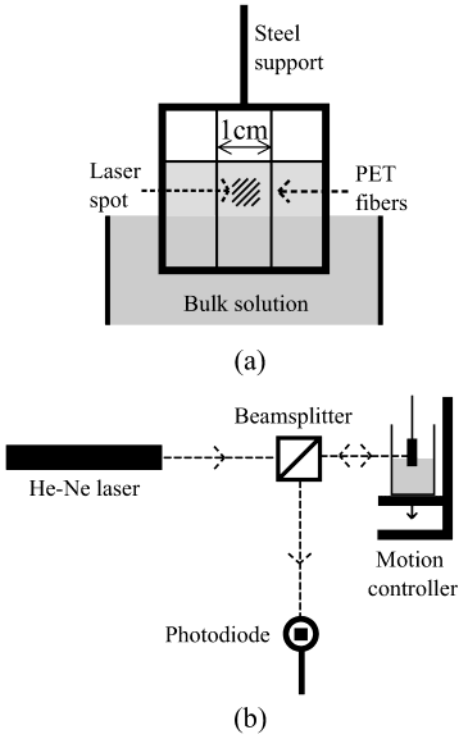

Figure 2. (a) Schematic diagram of the entrainment assembly. The PET fibers are held in place by an exterior steel support. (b) Schematic diagram of the optical assembly used in the laser interferometry experiments.

process. These values were estimated from $\dot{\gamma} \approx 2V_w/h_0$, where the film thickness h_0 was obtained from the interferometry data. The actual shear rates are smaller than these values since the film thickness in the meniscus region is much larger than h_0. Solutions without polymer produced film thicknesses in the range 0.3−15 μm; the addition of PEO produced films in the range 0.3−25 μm. In general, for the same value of capillary number, the films with polymer were thinner but exhibited longer drainage times before rupture.

C. Apparatus. An optically flat glass cell measuring 5 × 5 × 8 cm (depth) was partially filled with soap solution. The cell was mounted on a vertical stage attached to a single-axis motion controller (US Eurotek, CA) whose speed could be varied from 0.7 to 200 μm/s. As shown in Figure 2, a steel support was internally fitted with three 18-μm-diameter poly(ethylene terephthalate) (PET) fibers. Slender fibers tend to suppress significant capillary drainage at the top and sides of suspended films.[28] The vertical fibers were set 1 cm apart. This geometry produced three lateral films. The hatched symbols designate the portion of the central film used to extract the entrained film thickness. The experiment commenced by submerging the frame in solution above the level of the horizontal PET fiber. The liquid-filled cell was then programmed to move downward at constant speed. The external steel frame was held stationary and isolated from the motion controller by mounting it to an independent support. As the liquid level approached the cell bottom, the motion controller was stopped and the film continued to drain. Given the short overall travel distance, the majority of the interferometric data was collected after the translational motion had ceased.

Prior to each experimental run, the stainless steel frame was cleaned by immersion in a beaker containing a dilute solution of Contrad 70 (Decon Laboratories). The beaker was placed in an ultrasonic bath (Fisher Scientific FS140) at 50 °C for 1 h, then thoroughly rinsed in ultrapure water, and dried in a filtered stream of nitrogen gas. The PET fibers were strung by hand through small holes in the steel frame to form a taut support. Significant care was required to avoid kinks or breakage of the fibers. This assembly was cleaned by sonication for 20 min, thoroughly rinsed in ultrapure water, dried in a filtered stream of nitrogen gas, and placed in a desiccator until further use.

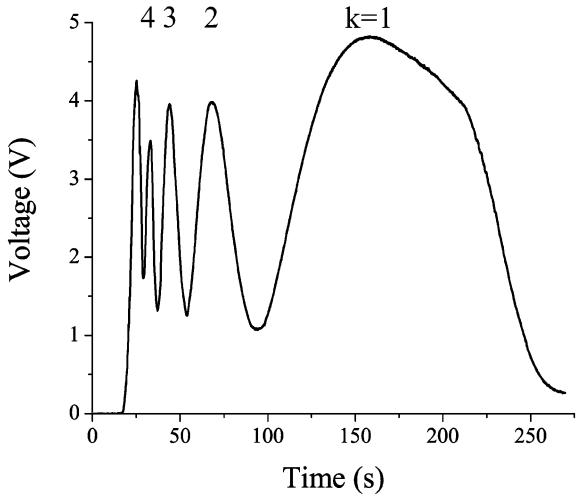

Figure 3. Voltage signal obtained during film drainage and thinning. The peaks used to back-count the initial film thickness are labeled as shown. The two sets of data, corresponding to film entrainment at 179 μm/s and $Ca = 4.56 \times 10^{-5}$ for solutions containing 2 wt % SDS and 2 wt % glycerol, are quite reproducible.

Previous researchers have noted difficulties in producing stable soap films. The PET fibers produced rather consistent and stable films; fibers made of nylon, copper, gold, and nickel−chromium alloy, which were cleaned in similar fashion, did not produce stable films as easily. Other types of exterior film supports were investigated to reduce the time-consuming task of manually stringing the slender fibers onto the steel frame. For example, the interior of thin rectangular blocks of both Teflon and Delrin were machined to remove a large central rectangular block. The interior edges were tapered to a sharp and smooth edge to support the formation of a soap film. In many instances, small edge asperities caused premature bursting of the films. This design, as well as others which suffered from edge roughness or chemical heterogeneities incurred after repeated use, were abandoned in favor of the fiber frame.

Soap films are also known to burst rather easily when subjected to small convection currents or evaporation. The glass cell containing the soap solution was therefore sealed with Parafilm, which was perforated at the center to accommodate the steel rod support. The entire apparatus, including the steel frame support and motion controller assembly, was enclosed within a large plastic container and mounted on a vibration-isolation optical table. The enclosure interior was humidified with a small water-filled vessel. The sealed glass cell was allowed to equilibrate in the humidified environment for approximately 4 h prior to an experimental run.

D. Optical Assembly. The thickness of the films entrained at constant speed was obtained with laser interferometry measurements. A schematic diagram of the optical assembly is shown in Figure 2b. Light from a He−Ne laser (Uniphase, 10 mW, $\lambda = 632.8$ nm) traveled through a 50/50 beam splitter striking the soap film at normal incidence. The illuminated spot was located at a distance of several millimeters below the horizontal PET fiber. The reflected light was made to impinge on a photodiode (Thorlabs PDA55 with amplified silicon detector). The voltage output indicated the reflected intensity as a function of time. To avoid saturating the photodiode, a neutral density filter was sometimes interposed between the laser and beam splitter. The voltage signal was used to reconstruct the entrained film thickness in the flat film region, as described below.

Curves of the reflected light intensity obtained in this way exhibit strong oscillations in time corresponding to conditions of constructive and destructive interference as the film drains and thins. Figure 3 shows two sample measurements of the recorded voltage for an aqueous solution containing 2 wt % SDS and 2 wt % glycerol at a withdrawal speed of $V_w = 179$ μm/s. For comparison with Frankel's law, it is necessary to determine the entrained film thickness prior to drainage for each withdrawal speed. This

comparison assumes that the measurements are extracted from the flat film region (see Figure 1).

The films eventually thin toward the black film (near $k = 1$) limit, where the thickness is below one-quarter of the wavelength of visible light,[36] reaching a metastable equilibrium thickness before finally bursting. Measurements of the initial film thickness can be obtained by enumerating the fringes formed prior to the black film limit. The film thickness corresponding to each maximum in the voltage curve, $V(t)$, is given by

$$h_{\max} = \frac{\lambda}{4n} + \frac{\lambda(k-1)}{2n} \tag{3}$$

where λ is the wavelength of the incident light, k is the order of the fringe labeled according to the numbering scheme in Figure 3, and n is the index of refraction of the solution. The film thickness corresponding to the minima preceding each fringe is given by $h_{\max} + \lambda/4n$. The initial film thickness can therefore be reconstructed from these drainage curves by counting the number of maxima and minima of the curves for $V(t)$.[37] At early times, the voltage signal rises rapidly to the first local maximum. To estimate correctly the corresponding increment in film thickness associated with this portion of the curve, we calculated the local rate of drainage from the two nearest extrema and linearly extrapolated the curve to $t = t_0$, the time at which a signal was first recorded. This increment in film thickness was negligible for all but the thinnest films.

Reflections from flat and parallel interfaces subject to a normal incident beam should produce voltage oscillations of constant amplitude. In practice, the oscillation amplitudes vary in time as shown in Figure 3; this behavior was also observed in Cohen-Addad's study.[24] Such variations can be due to several effects including deviations from normal incidence at times during which the film surfaces are not flat and parallel. A separate study[38] in our laboratory has combined similar interferometric studies with digital video images of the *entire* film surface during entrainment. While instabilities reminiscent of marginal regeneration are observed along all the film borders, the fluctuations in film thickness are rather small and sufficiently far from the measurement area to produce no noticeable fluctuations in $V(t)$. They also do not seem to affect the number of fringes generated. In fact, soap films formed on either side of the main central film occasionally burst during a run. Even film disturbances as large as these caused by random bursting events did not affect the number of fringes formed within the central film. We concluded after sufficient study that the enumeration procedure used in reconstructing the value of h_0 was rather robust and reproducible.

III. Experimental Results

Figure 4 shows measurements of the initial film thickness (normalized by the capillary length $\sqrt{\gamma/\rho g}$) as a function of increasing capillary number for five different solutions. Three of the solutions contain no polymer; two solutions contain low M_w PEO (17.5K) at 2.0 and 5.0 wt %. The data span approximately 3 decades in capillary number ($10^{-6} \lesssim Ca \lesssim 10^{-3}$). Each data point in Figures 4−6 represents the average of 3−5 runs obtained at the same speed. The horizontal dotted line in Figures 4 and 5 denotes the diameter of a dry PET fiber normalized by $\sqrt{\gamma/\rho g}$, where $\rho = 1.0$ kg/m^3 and $\gamma = 39.2$ or 37.5 mN/m; see values in Table 1. Frankel's law is designated by the solid straight line. The agreement with Frankel's law is good; the data lie slightly above the Frankel prediction especially at higher values of Ca, where the film thickness approaches the fiber diameter. Data collection at the slowest speeds (small Ca) was limited by the fact that films smaller than $\lambda/2n$ do not generate a clear single fringe in $V(t)$. Fits to the PEO data according to $H \sim Ca^{\beta}$ yielded exponents β as large as 0.73−0.79, which is slightly larger than the Frankel result of 2/3. These findings are consistent with previous measurements of similar solutions.[22]

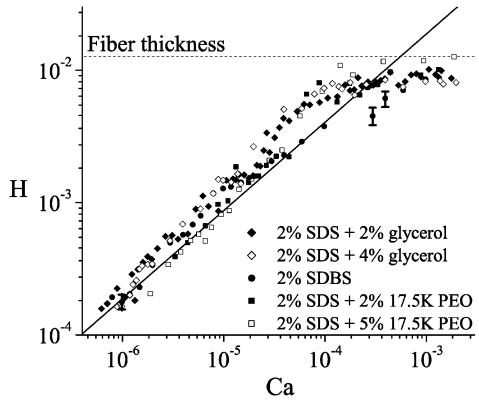

Figure 4. Results of the dimensionless film thickness, H, versus capillary number, Ca, for five solutions (only two containing low M_w PEO). The polymeric films exhibit slight deviation from Frankel's law (solid line). The dotted line represents the value of the fiber thickness normalized by the capillary length for $\gamma = 39.2$ mN/m. The three error bars shown represent the maximum deviations in film thickness in Ca for the 2 wt % SDBS solution. No systematic trends in measurement error were seen as a function of Ca.

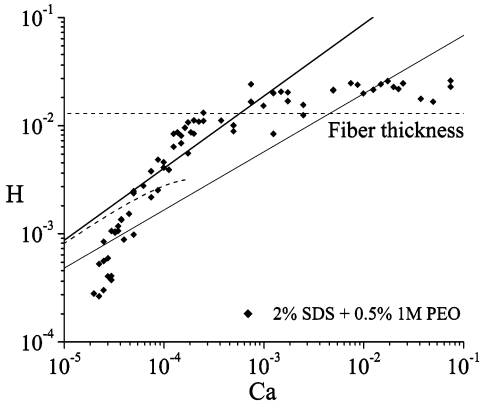

Figure 5. Measurement of the entrained film thickness (normalized by the capillary length) as a function of capillary number, Ca, for solutions consisting of 1M M_w PEO/SDS (0.5/2 wt %). Frankel's law is the upper solid line. The horizontal dashed line represents the value of the fiber thickness normalized by the capillary length for $\gamma = 37.5$ mN/m. The slope of the lower solid line corresponds to $2m/(2m + 1)$ (see eq 6) for $m = 0.68$. Even for an extremely long relaxation time $\lambda_r = 20$ s, the prediction of eq 7 (shown as the curved dashed line) does not capture the behavior of the data shown. Smaller and more realistic values of λ_r produce curves indistinguishable from Frankel's law.

By comparison, the normalized film thickness for aqueous SDS solutions containing 1M PEO at 0.5 wt % showed significant deviation from Frankel's law, as evident in Figure 5. There exists a much stronger dependence of the film thickness on Ca. At the higher withdrawal speeds, the film thickness exceeds the fiber diameter. The behavior of these solutions cannot be characterized by a simple power law over the range in capillary number shown.

A summary of all the results for solutions with polymer M_w ranging from 17.5K to 8M is shown in Figure 6. The

(36) Newton, I. *Opticks, or a Treatise of the Reflections, Refractions, Inflections & Colours of Light*, republication of the 4th ed. of 1730; Dover: New York, 1979; Book 2, Part 1.

(37) Born, M.; Wolf, E. *Principles of Optics: Electromagnetic Theory of Propagation, Interference and Diffraction of Light*, 2nd ed.; Macmillan: New York, 1964.

(38) Berg, S.; Adelizzi, E. A.; Troian, S. M. Experimental Study of Entrainment and Drainage Flows in Microscale Soap Films, submitted to *Langmuir*.

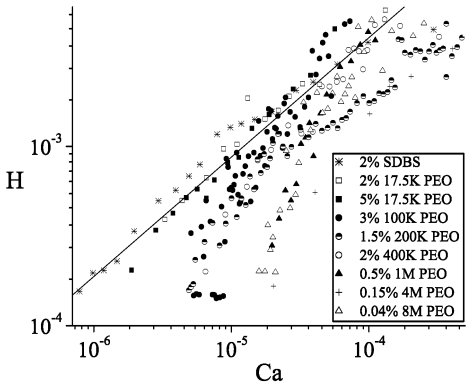

Figure 6. Complete results of the measured film thickness (normalized to the capillary length) as a function of capillary number, *Ca*, for solutions consisting of 2 wt % SDS and PEO molecular weights ranging from 17.5K to 8M. An additional aqueous solution only containing 2 wt % SDBS, which produces rigid films, is shown for comparison. Frankel's law is denoted by the solid line.

data show a clear deviation from Frankel's law with increasing M_w: solutions containing 1M, 4M, and 8M PEO lie far below the Frankel prediction, while those containing 400K, 200K, and 100K PEO lie progressively closer. The data also indicate that the strongest deviations occur at the smaller values of capillary number. It was not possible to access the same lower limit in *Ca* for all solutions because of the range in speed accessible to the motion controller and the range in solution viscosity. Except for the aqueous solutions containing only SDBS or SDS and low M_w polymer, none of the remaining data could be fit by a single exponent at the lower values of *Ca*.

To further characterize these liquid samples, we measured the shear-dependent viscosity (data not shown) and the first normal stress difference, N_1. The shear viscosity of the SDS−PEO solutions were well-fitted by the power-law relation $\tau = k\dot{\gamma}^m$, where τ denotes the shear stress within the fluid. The shear-dependent viscosity was fit by the form $\mu = k\dot{\gamma}^{m-1}$. Measurements of $\mu(\dot{\gamma})$ for the 1M SDS/PEO solutions, for instance, gave $\mu = 3.53\dot{\gamma}^{-0.32}$. All the soap solutions containing PEO exhibited shear-thinning behavior.

Pressure transducers on a Rheometrics Ares HR cone-and-plate rheometer were used to record the normal force, F_{N0}, exerted by the sheared liquid on the cone surface. These measurements were corrected for inertial forces, F_i, which thrust fluid from the gap region at sufficiently high shear rates.[39] The inertial correction was estimated from the relation

$$F_i = \frac{\pi\rho R^2\dot{\gamma}^2 h_e^{\,2}}{12} \tag{4}$$

Here, R is the radius of the cone and h_e is the gap width at the outer cone perimeter. The first normal stress difference, defined by $N_1 = \tau_{yy} - \tau_{xx}$, increases with shear rate as $N_1 = \Psi_1\dot{\gamma}^2$. The first normal stress coefficient, Ψ_1, was computed from the net normal force, $F_N = F_{N0} + F_i$, according to

$$\Psi_1 = \frac{2F_N}{\pi\dot{\gamma}^2 R^2} \tag{5}$$

(39) Bird, R. B.; Armstrong, R. C.; Hassager, O. *Dynamics of Polymeric Liquids*; John Wiley and Sons: New York, 1987; Vol. 1, Chapter 10.

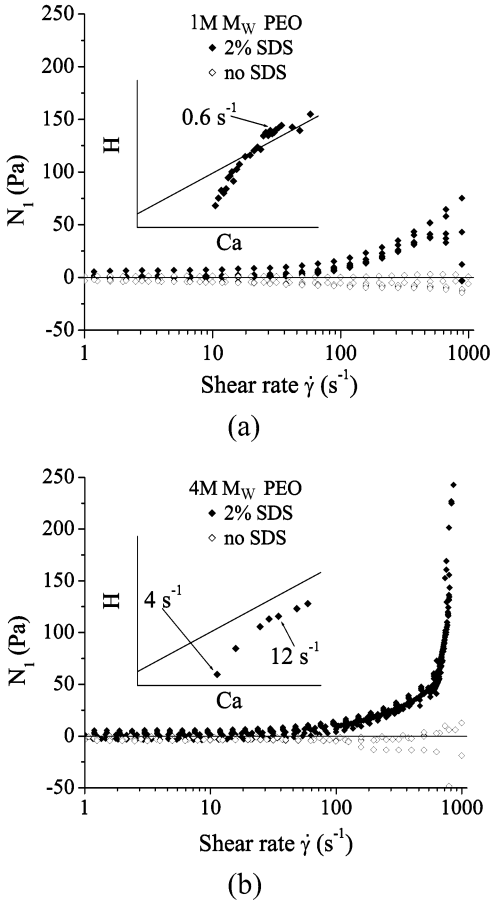

Figure 7. Measurements of the first normal stress difference, N_1, as a function of shear rate, $\dot{\gamma}$, for solutions consisting of (a) 1M M_w PEO and (b) 4M M_w PEO. Solid diamonds (♦) represent aqueous PEO solutions with 2 wt % SDS. Open diamonds (◊) represent aqueous PEO solutions with no SDS. The inset figures of film thickness versus capillary number show estimated shear rates produced during the film entrainment process.

Solutions containing polymer in the range $M_w \leq 400$K, with or without SDS, registered no discernible normal stress coefficients below 1000 s^{-1}. The higher M_w solutions produced measurable values of Ψ_1 above a sufficiently high shear rate. Figure 7 shows measurements for 1M and 4M PEO solutions with and without SDS. The different curves represent single runs through the full range in shear rate. In general, aqueous solutions of PEO containing no SDS produced negligible normal stresses, except for the highest molecular weight samples subject to the largest shear rates. Addition of SDS, however, causes a marked increase in Ψ_1. For example, aqueous solutions of 1M PEO (4M PEO) containing no surfactant showed vanishingly small normal stress coefficients below 1000 s^{-1} (300 s^{-1}). The addition of SDS caused a rise in Ψ_1 above 50 s^{-1}. Polymer−surfactant complexation is likely responsible for the enhanced normal stresses observed in the SDS/PEO solutions. This enhancement, however, is only significant for shear rates exceeding those accessible to the interferometric setup used in this study. The two insets in Figure 7 represent measurements of the film thickness versus capillary number for the corresponding SDS/PEO solutions. The values of the shear rates superimposed on the curves correspond to the (upper bound) estimates in shear rate given in Table 1. From these observations, we concluded that normal stress effects are not primarily responsible for the strong deviations from Frankel's law observed for these solutions.

IV. Hydrodynamic Models for Film Entrainment

Several theoretical models have been proposed to explain the dependence of the entrained film thickness on capillary number in associating surfactant−polymer solutions. Frankel's derivation assumes a Newtonian film with rigid interfaces. Several researchers have extended the original calculation to non-Newtonian fluids and replaced the boundary conditions corresponding to rigid interfaces by an effective slip condition. We review next the predictions of several of these models and make comparison to the experimental trends observed.

A. Rheological Effects. *1. Shear-Thinning Fluids.* A straightforward extension of the Frankel analysis to account for a power-law fluid described by $\tau_{yx} = k\dot{\gamma}_{yx}^{m}$, leads to the result[22,40]

$$H \sim V_w^{2m/(2m+1)} \tag{6}$$

Since all the polymeric−surfactant solutions in our studies exhibited shear-thinning behavior (i.e., $m < 1$), this prediction should generate a weaker dependence on Ca than observed with Frankel's law. The experimental results, however, show a stronger, not weaker, dependence on capillary number, especially at smaller values of Ca (see Figure 6). As discussed in section III, all the solutions are essentially Newtonian liquids at the shear rates of interest. Shear-thinning behavior cannot therefore explain the trends evident in Figure 6.

2. Purely Normal Stress Effects. Bruinsma et al. examined the consequence of normal stress effects in soap films slowly withdrawn from solution.[40] They assumed that, in the limit of extremely large normal stresses, viscous effects are negligible and the capillary pressure due to film curvature exactly balances the normal stress. Their derivation, while not completely consistent with a rigorous treatment of normal forces, led to the relation $H \sim [(\Psi_1\gamma\kappa)^{1/2}/\mu)]Ca$. The prediction that the entrained film thickness scales linearly with Ca is not supported by the data in Figure 6. This lack of agreement is not surprising since measurements of the SDS/PEO solutions showed no significant normal stresses at the shear rates accessible to the film entrainment assembly.

3. Viscoelastic Effects. Ro and Homsy examined the behavior of (linear) viscoelastic free surface flows at low capillary number for Hele-Shaw and dip-coating geometries.[41] They used a constitutive equation corresponding to an Oldroyd B fluid and retained approximations to describe shear thinning and normal stress effects. The analysis was formulated as a double expansion in the two small parameters $Ca^{1/3}$ and $We{\cdot}Ca^{1/3}$, where the Weissenberg number $We = \lambda_r V/\sqrt{\gamma/\rho g}$ is directly proportional to λ_r, the polymer relaxation time. Their final result was given by

$$H = 1.89Ca^{2/3} - 0.189Ca^{1/3}We + ... \tag{7}$$

The two mechanisms controlling the film thickness in their studies were shown to be the resistance to streamwise strain, which reduces the entrained thickness, and the buildup of shear stress, which increases it. When the viscoelastic effect dominates the streamwise strain, the entrained film thickness scales as $V^{4/3}$, as evident from the second term on the right in eq 7. Extension of this result to soap film entrainment predicts that $H \sim V_w^{4/3}$, a stronger dependence on capillary number than Frankel's law.

Direct comparison of this prediction with experiment requires an estimate of the polymer relaxation time, which in our case is increased by complexation effects. Polymer relaxation with associative, electrostatic, or covalent effects is poorly understood and there are currently no models which incorporate these effects. As a first approximation, these complexation effects can be ignored and λ_r estimated by assuming that the polymer is in a good solvent (as true for PEO in water with no SDS) and behaves as an ideal Rousian chain. Accordingly, the relaxation time is given by

$$\lambda_r = \frac{[\mu]_0/\mu_s M_w}{RT} \tag{8}$$

where $[\mu]_0$ denotes the intrinsic viscosity, μ_s the solvent viscosity, R the gas constant, and T the temperature.[42] The Mark−Houwink relation provides an estimate of the intrinsic viscosity $[\mu]_0 = KM_w^a$ where K and a are empirically determined constants. For PEO in water ($10^4 \le M_w \le 10^7$), these constants have been measured to be $K = 1.25 \times 10^{-4}$ and $a = 0.78$.[43,44] Chari et al.[35] measured the value a for PEO saturated with SDS to find a slightly larger constant ($a = 0.94$). According to these approximations then, an estimate of the relaxation time for a 1M M_w PEO solution would be on the order of 10^{-2} s. Incorporation of this estimate leads to numerical solutions for H versus Ca that are indistinguishable from Frankel's law. Polymer association and coil elongation due to bound surfactant micelles is expected to increase the polymer relaxation time; however, an increase in λ_r by over 2 orders of magnitude over the Rouse estimate still shows no discernible deviation from Frankel's law below $Ca \sim 10^{-3}$. Excessively large and unphysical estimates of the relaxation times, as shown in Figure 5 for $\lambda_r = 20$ s, leads to saturation of the entrainment curves for increasing values of Ca. We conclude that weak viscoelastic and normal stress effects therefore cannot explain the trends observed with SDS/PEO solutions.

B. Interfacial Slip. Frankel's law describes the behavior of rigid soap films, for which it is assumed that the speed of the film surfaces $y = \pm h(x, t)$ exactly equals the film withdrawal speed V_w. This boundary condition is the analogue of the no-slip condition for liquid-on-solid systems. Bruinsma et al. were the first to modify Frankel's law by incorporating a Navier slip condition at the bounding surfaces.[40] This modification was intended to describe the behavior of mobile films whose surface velocity is different from the withdrawal velocity.

The native surface motion in mobile films is attributed to inhomogeneities in the surface surfactant concentration, $\Gamma(x)$, which produce Marangoni stresses.[3−5] The corresponding surface speed for thin films is given by

$$u[x, y = \pm h(x)] = \frac{h(x)}{\mu}\frac{\partial\gamma}{\partial\Gamma}\frac{\partial\Gamma}{\partial x} \tag{9}$$

Solution of the interfacial shape, $h(x)$, however, requires solution of an additional set of equations for the surfactant bulk $c(x, y)$ and surface profiles, which in turn depend on

(40) Bruinsma, R.; di Meglio, J.-M.; Quéré, D.; Cohen-Addad, S. *Langmuir* **1992**, *8*, 3161.

(41) Ro, J. S.; Homsy, G. M. *J. Non-Newtonian Fluid Mech.* **1995**, *57*, 203.

(42) De Gennes, P.-G. *Scaling Concepts in Polymer Physics;* Cornell University Press: Ithaca, NY, 1979.

(43) Bailey, F. E., Jr.; Koleske, J. V. *Poly(ethyelene oxide)*; Academic Press: New York, 1976.

(44) Bailey, F. E., Jr.; Kucera, J. L.; Imhof, L. G. *J. Polym. Sci.* **1958**, *32*, 517.

the equation of state relating the surface tension γ to Γ. Realistic equations of state are difficult to obtain even for pure aqueous surfactant solutions. While this approach has been used to solve the modified Bretherton problem,[45] there is still difficulty in making exact comparison to experiment.

From a hydrodynamic point of view, little is really known about the modification in surface flow resulting from polymeric additives, especially in systems subject to complexation. The polymer can act as a physical barrier to surfactant adsorption/desorption, thereby causing a depletion of surfactant in the meniscus region as surface area is generated during the withdrawal process. This effect would cause a downward Marangoni flow and thinner entrained films. Surfactant−polymer complexation might also lead to phase separation within the film whereby the interior bulk phase slips against the exterior phase during entrainment. This effect would also generate thinner films. As shown earlier in section III, the addition of high M_w polymer, even at very low concentrations, causes strong deviations from Frankel's law unexplained by viscoelastic effects. The overall trend, however, points to thinner films especially at the smallest capillary numbers. The approach detailed below assumes that to first order it is possible to parametrize these possibilities as an effective slip condition at the gas−film interface.

Bruinsma et al. were the first to show that the entrainment behavior of SDS/PEO solutions for 4M M_w was well-capturerd by a modified Frankel model in which the no-slip condition was replaced by the Navier slip condition.[40] Unfortunately, these authors eventually abandoned this explanation since the inferred slip lengths seemed far too large when compared with estimates from molecular models based on polymer melts. It is now known, however, that fluid−fluid interfaces can give rise to slip lengths in the micrometer range, especially in polymeric systems. We briefly review current evidence of slippage in a number of systems and outline the original modification to Frankel's analysis for interfacial slip.[40]

1. Slip at Liquid−Solid and Polymer Melt Interfaces. As early as 1823, Navier conjectured that, for sufficiently high shear rates, liquid molecules can slip past a stationary solid substrate. He proposed to replace the classical no-slip condition[46,47] by the boundary condition $V_{slip} = b\dot{\gamma}$, where the slip length b was defined as the extrapolation length into the solid phase where the velocity field vanishes. In his original analysis, the slip length was assumed to be independent of the local shear rate. More recent models[48] and molecular dynamics simulations[49,50] indicate how the slip length can vary with increasing shear rate.

Slippage at smooth and rough interfaces, which is normally established above a critical shear rate, has been deduced from numerous studies involving simple liquids, polymer solutions, and polymer melts.[51−53] The shark skin texture observed in extruded polymer melts, for example, is known to be caused by multiple and successive adhesive and slip events at the melt−solid interface.[54] In general, however, it is difficult to measure slip lengths directly and most measurements must still rely on some model where the slip length is treated as an adjustable parameter. For example, in recent studies of Boger liquids in squeeze flow using a surface force apparatus, Horn et al.[55] have estimated slip lengths on the order of the 30−50-nm range for shear rates in the range $1 \leq \dot{\gamma} \leq 100\ s^{-1}$. The squeeze flow enforces film thinning and drainage between two locally flat mica sheets separated by distances ranging from 10^3 to 30 nm. A simple Navier slip condition was used to infer these values. Zhu and Granick have also used a modified surface force apparatus to study the slip behavior of liquids such as water and tetradecane against smooth and rough surfaces.[56] Substrates treated with organic monolayers forming hydrophobic surfaces produced the largest slip response; water films squeezed between OTE-coated mica surfaces generated slip lengths on the order of the decreasing gap size.

Much larger slip lengths have been reported in high molecular weight polymer melts. Zhao and Macosko have investigated slip effects in coextruded multilayer samples of polypropylene(PP)/polystyrene (PS) and polystyrene (PS)/poly(methyl methacrylate) (PMMA).[57] In both cases, the apparent viscosity, as measured by an in-line slit rheometer and a parallel plate rheometer, decreased with increasing number of layers, thereby indicating interfacial slip between adjacent polymer layers. Extraction of the slip velocity was obtained by analysis for coextrusion using an Ellis model; slip lengths approached 10 μm. When a premade diblock copolymer was allowed to diffuse across the PP/PS interfaces, interfacial slip was suppressed. Models of weakly incompatible polymer−polymer melt interfaces also suggest that the reduction in polymer entanglements and the subsequent decrease in viscosity within the interfacial region can lead to substantial slip.[58] For $\dot{\gamma} > 1000$ Pa, the slip velocity was found to increase linearly with shear rate for speeds in the range 0.01−10 μm/s. Archer et al. measured the degree of slip in polystyrene−(tricrecyl phosphate) solutions flowing past glass substrates in simple Couette flow.[59] By observing the motion of micrometer-sized silica spheres, they deduced velocity profiles in the vicinity of the solid substrates consistent with slip lengths as large as 40 μm even for shear rates as small as $0.01 < \dot{\gamma} < 0.25\ s^{-1}$. Significant slip lengths have also been reported in polybutadiene[60,61] and polystyrene melts.[62]

Tretheway and Meinhart have used micrometer-resolution particle image velocimetry to measure the velocity profile of water flowing through glass capillaries.[63] While uncoated glass substrates produced velocity profiles consistent with the no-slip condition, water flowing against OTS (octadecyltrichlorosilane)-coated glass substrates generated slip lengths on the order of a micrometer.[63] Water films against a hydrophobic surface, however, pose a special problem. Recent studies indicate that slightly acidic, un-degassed water against a hydrophobic glass substrate can produce a dense layer of elongated nanobubbles which nucleate at the liquid−solid surface.[64] These nanobubbles appear to enhance slip by forming an

(45) Ratulowski, J.; Chang, H. C. *J. Fluid Mech.* **1990** *210*, 303.
(46) Navier, C. L. M. H. *Mem. Acad. R. Sci. Inst. Fr.* **1823**, *6*, 389.
(47) Goldstein, S., Ed. *Modern Developments in Fluid Mechanics*; Oxford University Press: New York, 1938.
(48) Greenspan, H. P. *J. Fluid Mech.* **1978**, *84*, 125.
(49) Thompson, P. A.; Troian, S. M. *Nature* **1997**, *389*, 360.
(50) Priezjev, N. V.; Troian, S. M. *Phys. Rev. Lett.* **2004**, *92*, 018302.
(51) Mooney, M. *J. Rheol.* **1931**, *2*, 210.
(52) Reiner, M. *J. Rheol.* **1931**, *2*, 337.
(53) De Gennes, P.-G. *C. R. Acad. Sci. Paris Ser. 2* **1979**, *288*, 219.
(54) Denn, M. M. *Annu. Rev. Fluid Mech.* **2001**, *33*, 265.
(55) Horn, R. G.; Vinogradova, O. I.; Mackay, M. E.; Pan-Thien, N. *J. Chem. Phys.* **2000**, *112*, 6424.
(56) Zhu, Y.; Granick, S. *Phys. Rev. Lett.* **2002**, *88*, 106102.
(57) Zhao, R.; Macosko, C. W. *J. Rheol.* **2002**, *46*, 145.
(58) Brochard-Wyart, F.; de Gennes, P.-G.; Troian, S. M. *C. R. Acad. Sci. Paris Ser. 2* **1990**, *310*, 1169.
(59) Archer, L. A.; Larson, R. G.; Chen, Y.-L. *J. Fluid Mech.* **1995**, *301*, 133.
(60) Mhetar, V.; Archer, L. A. *Macromolecules* **1998**, *31*, 8607.
(61) Mhetar, V.; Archer, L. A. *Macromolecules* **1998**, *31*, 8617.
(62) Henson, D. J.; Mackay, M. E. *J. Rheol.* **1995**, *39*, 359.
(63) Tretheway, D. C.; Meinhart, C. D. *Phys. Fluids* **2002**, *14*, L9.
(64) Tyrrell, J. W. G.; Attard, P. *Phys. Rev. Lett.* **2001**, *87*, 176104.

interstitial layer near the solid wall with ultralow viscosity due to the high gas content.[65,66]

2. Slip in Associating Surfactant−Polymer Films. The majority of slip studies have focused almost exclusively on liquid−solid or polymer−polymer interfaces. Bruinsma et al.[40] and Cohen-Addad,[24] however, were perhaps the first to consider the possibility of interfacial slip in associating polymer-surfactant solutions. They assumed that the interior liquid film, which consists of polymer−micelle aggregates, can slip against the exterior interface made rigid by an excess of surfactant. While there are no available measurements relating to the structures formed by associating polymer−surfactant aggregates at the air−liquid interface, Chari has described how surface micelles consisting of SDS clusters can link to polymer chains near the interface.[67] He inferred the existence of such a micelle layer from examining the adsorption behavior and surface tension of aqueous solutions of poly(vinylpyrrolidone) (PVP) and SDS. As we discussed in section I, further study is required to identify the source of interfacial slip in such systems. Nonetheless, it proves useful for these and other systems[38] to postulate the existence of an effective slip behavior at the boundary surfaces.

Frankel's original derivation can be modified[40] by inclusion of the Navier slip condition (see Figure 1) according to

$$V_{y=h} = V_w - V_{slip} = V_w - b\left(\frac{\partial u}{\partial y}\right)_{y=h} \tag{10}$$

which when incorporated into a steady-state lubrication analysis leads to the evolution equation for the dimensionless film thickness, $H = h(x)/h_0$:

$$H_{XXX} = \frac{1 - H}{H^3 + \frac{3b}{h_0}H^2} \tag{11}$$

Here, h_0 represents the uniform film thickness far from the meniscus region and X denotes the dimensionless streamwise coordinate

$$X = \frac{x}{h_0}(3Ca)^{1/3} \tag{12}$$

The Frankel relation in eq 1 is recovered in the limit $b \rightarrow 0$.[24,40]

To compare our experimental data with predictions of the entrained film thickness, eq 11 was solved by a standard shooting technique using a fourth-order Runge−Kutta algorithm. The equation for the film profile was obtained by integrating away from the flat film region toward the meniscus region until the curvature H_{XX} was found to be constant.[2] To improve convergence, the slope and curvature in the flat film region were determined from a linearization of eq 11 about $H = 1$.[2,15] Mesh refinement and overall size of the domain of integration were varied to test convergence and stability. The slip length, b, was treated as an adjustable parameter when fitting the experimental data to the numerical solutions. Figure 8 demonstrates the effect of increasing slip length for values ranging from 10^{-2} to 10^4 μm. Small values of b generate curves almost indistinguishable from Frankel's law. Larger values produce films whose thickness is much smaller than the original Frankel's law especially at the smaller values of Ca, as observed in Figure 6. For slip lengths which far exceed h_0, eq 11 predicts that $H \sim Ca^2$, as confirmed in Figure 6. Figure 9 shows a comparison of the numerical solutions to the experimental data for SDS/PEO solutions. The slip lengths for aqueous SDS/PEO solutions with polymer M_w in the range 17.5K−8M (see Table 1) range from 0.2 to 8 μm and increase with M_w. The data points shown in Figure 9 represent measurements from individual runs at fixed withdrawal speed. The variability in film thickness evident for fixed values of the capillary number provides an estimate of the overall measurement error. Despite the scatter in the data, comparison to the trends predicted by the slip model consistently describes the progressively larger deviations from Frankel's law for decreasing capillary number, unlike the predictions of models discussed earlier in section IV. A.

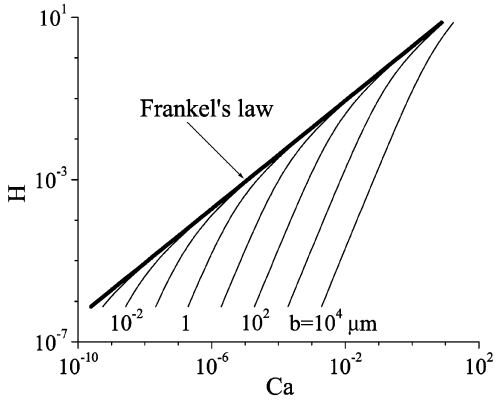

Figure 8. Numerical solutions of eq 11 for slip lengths ranging from 10^{-2} to $10^4\mu$m. The larger the slip length, the stronger the deviation from Frankel's law. In the limit where the slip length exceeds the film thickness, $H \sim Ca^2$, as previously shown.[24,40]

3. Tolstoi Slip Model. In 1952, Tolstoi developed a phenomenological model,[25,26] based on the molecular kinetic theory of Frenkel,[68] describing how the slip length for *simple fluids* adjacent to a flat, solid wall should correlate linearly with the molecular size of the fluid phase. He treated the motion of liquid molecules subject to a constant stress as a biased activated (Eyring) process. In this way, he was able to correlate the activation enthalpy for molecular motion near the wall to the work of adhesion and cohesion with the result

$$b = a\left(\frac{\mu}{\mu_w} - 1\right) \tag{13}$$

where a represented the diameter of the molecules in the liquid phase, μ the bulk liquid viscosity, and μ_w the reduced viscosity of the first liquid layer near the wall.[25,26] This relation therefore suggested that a reduction in μ_w by an order of magnitude from the bulk viscosity could produce slip lengths in the range of 1−100 nm. Larson[27] extended this line of reasoning to polymer melts near a solid wall by assuming that a represents the polymer radius of gyration $R_g \sim M_w^{1/2}$. Polymer entanglements, which are suppressed near the wall for weakly adsorbing species,[69] can lead to huge ratios μ/μ_w, resulting in slip lengths on the order of 1000a. Further extension of Larson's model to a dilute polymer solution in a good solvent including excluded-volume effects predicts that $a \sim \langle R^2\rangle^{1/2} \sim M_w^{3/5}$. (While Tolstoi's model assumes that the solvent and solute

(65) Bingham, E. C. *Fluidity and Plasticity*; McGraw-Hill: New York, 1922.
(66) De Gennes, P.-G. *Langmuir* **2002**, *18*, 3413.
(67) Chari, K. *J. Phys. II Fr.* **1995**, *5*, 1421.
(68) Frenkel, J. *Kinetic Theory of Liquids*; Oxford University Press: New York, 1946.
(69) Brochard, F.; de Gennes, P.-G. *Langmuir* **1992**, *8*, 3033.

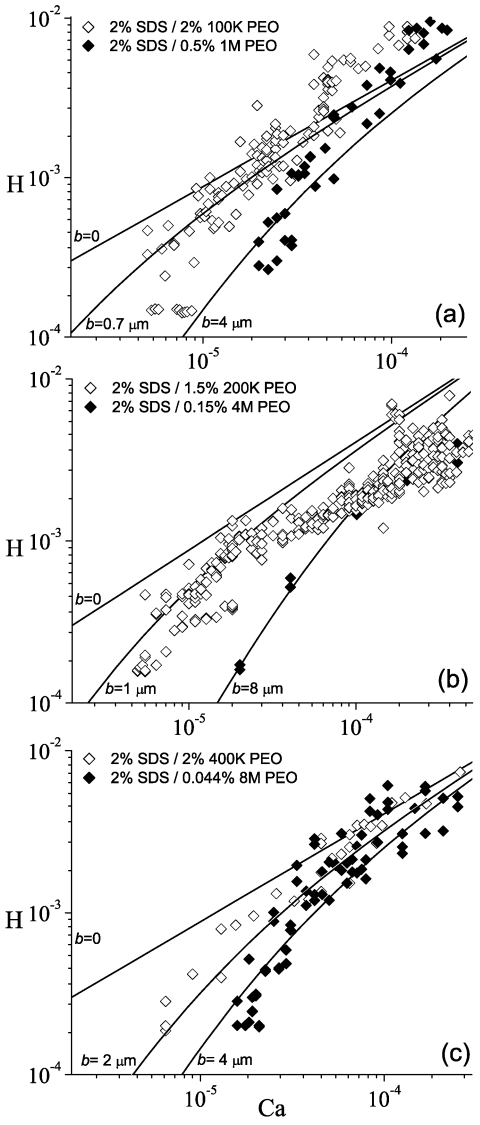

Figure 9. Comparison of the slip model (solution to eq 11) to interferometric data for the entrained film thickness. The curves labeled by $b = 0$ represent the Frankel prediction for rigid films (i.e., no slip). (a) 100K PEO (open diamonds (◊)) and 1M PEO (solid diamonds (♦)); (b) 200K (◊) and 4M PEO (♦); (c) 400K (◊) and 8M PEO (♦). Data are not averaged; the spread of thickness data for each *Ca* is an indication of the uncertainty of the measurements.

Table 2. Numerically Extracted Slip Length for Soap Films with 2 wt % SDS and PEO Molecular Weights Ranging from 17.5K to 8M[a]

M_w	b (μm)	M_w	b (μm)	M_w	b (μm)
17.5K	0.2	400K	2	4M	8
100K	0.7	1M	4	8M	4
200K	1				

[a] These data are plotted in Figure 10.

molecules are of the same size, an alternative relation in Frenkel's analysis can be applied to macromolecules in solution with the identical result shown in eq 13.)

As originally derived, the Tolstoi−Larson model applies exclusively to fluid−solid interfaces and not fluid−fluid interfaces as exist in freely suspended films. Nonetheless, in the absence of any alternative models, we investigated the molecular weight dependence of the slip lengths inferred from the modified Frankel analysis. Table 2 contains a list of the slip lengths extracted from the experimental data as a function of the polymer molecular

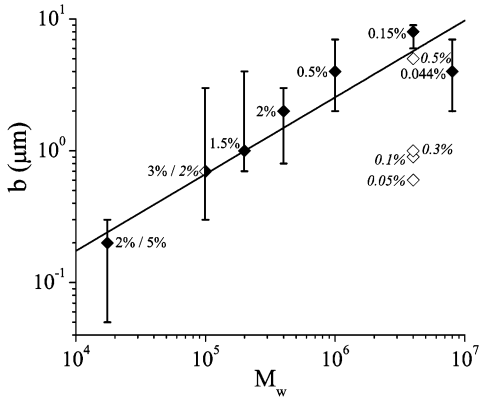

Figure 10. Correlation between the extracted slip length, b, and the polymer molecular weight, M_w, for SDS/PEO films. Solid diamonds (♦) are results from Figure 9. Open diamonds (◊) are our fits to the data of Cohen-Addad.[22,24] The solid line represents the best linear fit.

weight for all the SDS/PEO solutions used in this study. The slip lengths generally increase with polymer molecular weight as shown in Figure 10. The solid line represents a least-squares fit to the data with the correlation

$$b \sim M_w^{0.58\pm0.07} \tag{14}$$

Although it may only represent a coincidental result, it is interesting to note that the extracted exponent lies close to a value of 3/5. The measured slip length for the solution 17.5K M_w PEO lies slightly below the best fit line. Chari et al. have reported that PEO solutions of low molecular weight (M_w < 30K) exhibit the same diffusion coefficient in water with or without surfactant.[70] This behavior suggests little or no association between the polymer and surfactant. If this data point is excluded, then the slip length correlation is instead given by $b \sim M_w^{0.49}$, closer to an exponent of 1/2. Overall, the strong correlation between the slip length and the polymer size in these experiments suggests the presence of weak bulk−surface interactions and significant effective slip.

C. Marangoni Effects. Since SDS micelles are known to associate with PEO molecules in an aqueous environment, it is possible that the resulting aggregates somehow generate surface tension gradients at the boundary surfaces either by establishing an effective barrier to surfactant adsorption/desorption or by adsorbing nonuniformly at the air−liquid interface. For example, there is significant interfacial area continuously produced in the meniscus region during entrainment. If this region maintains a higher surface tension than the surrounding areas, there will occur an additional downward liquid flux due to Marangoni stresses. While these concentration gradients normally equilibrate rapidly for solutions above the CMC, complexation with polymer strands can slow the movement of surfactant micelles, thereby generating Marangoni effects even above the CMC. Ongoing work in our laboratory[38] has shown that pure aqueous surfactant solutions (no polymeric additives) below the CMC, where Marangoni effects are presumed significant, are also well-described by eq 11 with comparatively smaller slip lengths. The approach taken in this current study is that such complicated effects in polymer−surfactant solutions can nonetheless be effectively parametrized by a slip length. The correlation of the slip length with polymer molecular weight also seems consistent with the phenomenological Tolstoi−Larson model for fluid slip against rigid surfaces.

(70) Chari, K.; Antalek, B.; Minter, J. *Phys. Rev. Lett.* **1995**, *74*, 3624.

V. Conclusions

We have measured the thickness of soap films entrained on a slender fiber frame at small and constant speeds using laser interferometry. Pure soap films containing aqueous solutions of SDBS and SDS with glycerol (both above the CMC) confirm Frankel's law for rigid Newtonian films. Films containing a polymeric additive, PEO, which is known to associate with SDS micelles in an aqueous medium, generate progressively larger deviations from Frankel's law with increasing polymer molecular weight and decreasing capillary number.

Comparison of the experimental data for the film thickness to predictions of various hydrodynamic models incorporating shear thinning and normal stress effects shows poor agreement. Generalization of Frankel's analysis to include a slip boundary condition produces much better agreement. The extracted slip lengths are found to scale with polymer molecular weight according to M_w^{ζ} where $\zeta = 0.58 \pm 0.07$. We discuss these results in the context of a phenomenological model for slip against a rigid surface first derived for fluid−solid boundaries by Tolstoi for simple fluids[25] and later extended by Larson to polymer melts.[27]

Additional studies will be needed to isolate the primary mechanism leading to this effective slip behavior in freely suspended films. Experimental studies of the slip length at fixed polymer M_w but increasing concentration are currently underway. Studies which compare the entrained film thickness and extracted slip length as a function of the degree of complexation between polymer and surfactant will reveal more information about the correlation between slip and associative behavior. Hydrodynamic models incorporating both viscoelastic and Marangoni stresses in dip-coating flows will also help advance the simple concepts introduced here.

Acknowledgment. The authors gratefully acknowledge financial support from Unilever Research US, the National Science Foundation (CTS and DMR), and the Princeton Center for Complex Materials. The authors also wish to thank the Unilever scientific staff, including Dr. Alex Lips and Dr. Quynh Pham, for helpful discussions and use of the Rheometrics Ares HR Rheometer. Dr. Yash Kamath of TRI/Princeton kindly provided the PET fibers. The authors also thank Dr. Steffen Berg for kind assistance and interesting discussions.

LA035480X